Quantum Chemistry Computation of Rate Constants for Reactions Involved in the First Aromatic Ring Formation

Carlo Cavallotti,* Renato Rota,* and Sergio Carrà

Politecnico di Milano, Dip. di Chimica, Materiali e Ingegneria Chimica/CIIRCO, Via Mancinelli 7, I20131 Milano, Italy

Received: April 10, 2002; In Final Form: June 14, 2002

The formation of the first aromatic ring plays an important role in defining the chemical reaction pathways responsible for polycyclic aromatic hydrocarbon (PAH) and soot formation. In this work, the relative importance of *cyclo*-C_5 species formation with respect to the *cyclo*-C_6 one from the attack of vinyl radical on 1,3-butadiene has been investigated through quantum Rice−Ramsperger−Kassel (QRRK) theory and quantum chemistry. A fast and accurate method, which differs from the standard G2MP2 method in that geometries were optimized with B3LYP/6-31G(d,p), has also been proposed and validated. Kinetic constants for each elementary process involved in the reaction mechanism were determined with conventional transition-state theory. It has been found that the rate of formation of $C_5H_6^{c5}$ is always larger than that of $C_6H_8^{c6}$ in the whole temperature range investigated (that is, 500−2000 K). All of the results presented in this work lead to the conclusion that the reaction paths involving *cyclo*-C_5 species cannot be neglected in the detailed kinetic modeling of combustion processes when the first aromatic ring formation is involved.

1. Introduction

Nowadays, fossil fuels combustion is the main source of power for humanity. This will be also true in the near future because alternative energy sources cannot play a significant role in the next decades, thus enlarging the problems due to the atmospheric pollutants emission.[1] In particular, over the past several years attention has been focused on the emission of harmful airborne species, such as polycyclic aromatic hydrocarbons (PAH) and soot.[2]

The emission control of the harmful combustion products calls for the development of cleaner combustion devices. This will be possible only on the basis of a better physical and chemical understanding of the combustion processes. Although many important details of the PAH and soot formation are not completely understood, there is a general agreement on the main feature of the processes involved, and they have been recently reviewed by Richter and Howard.[3] The process starts with the formation of molecular precursors of soot (most probably heavy PAHs of molecular weight 500−1000 amu), followed by the nucleation from heavy PAHs (where mass is converted from molecules to particles of about 2000 amu molecular mass and 1.5 nm diameter) and by the growth of particles through the addition of gaseous molecules or the reactive particle−particle collision. However, the soot formation mechanism strongly depends on the operating conditions. For instance, it has been recently proposed that in slightly sooting flame conditions the soot formation occurs through the rearrangement of a large amount of transparent (in the visible) particles that are formed by fast reactions among small PAHs before soot inception.[4]

In any case, PAH formation proceeds through lighter aromatic compounds. Therefore, the formation of the first aromatic ring plays an important role in defining the chemical reaction pathways responsible for soot formation. Among others, benzene is an important intermediate.

A possible benzene formation channel involves the attack of vinyl radical on 1,3-butadiene or the 1,3-butadienyl radical attack on acetylene, both followed by hydrogen elimination:[5−8]

$$C_2H_3 + 1,3\text{-}C_4H_6 \leftrightarrow n\text{-}C_6H_9 \leftrightarrow c\text{-}C_6H_9 \leftrightarrow c\text{-}C_6H_8 + H \leftrightarrow \text{benzene} + H_2 + H \quad (1)$$

$$C_2H_2 + 1,3\text{-}C_4H_5 \leftrightarrow n\text{-}C_6H_7 \leftrightarrow c\text{-}C_6H_7 \leftrightarrow \text{benzene} + H \quad (2)$$

$$C_2H_2 + 1,3\text{-}C_4H_5 \leftrightarrow n\text{-}C_6H_7 \leftrightarrow \text{benzene} + H \quad (3)$$

1,3-Butadienyl radical can be formed by vinyl radical addition to acetylene:

$$C_2H_3 + C_2H_2 \leftrightarrow 1,3\text{-}C_4H_5 \quad (4)$$

A second possible pathway involves the recombination of propargyl radical:[9]

$$2C_3H_3 \leftrightarrow c\text{-}C_5H_4{=}CH_2 \leftrightarrow \text{benzene} \quad (5)$$

while propargyl radical can be formed by CH_2 radical addition to acetylene:

$$CH_2 + C_2H_2 \leftrightarrow C_3H_3 \quad (6)$$

An alternative path to benzene involves ethylene attack to cyclopentadiene:[10]

$$C_2H_4 + c\text{-}C_5H_6 \leftrightarrow \text{benzene} + H + CH_3 \quad (7)$$

where a route to cyclopentadiene is again from the attack of vinyl radical on 1,3-butadiene:[11]

$$C_2H_3 + 1,3\text{-}C_4H_6 \leftrightarrow n\text{-}C_6H_9 \leftrightarrow c\text{-}C_5H_6 + CH_3 \quad (8)$$

Unfortunately, despite the extensive work on the chemical reactions leading to the first aromatic ring, there is not yet a

* To whom correspondence should be addressed.

10.1021/jp025922y CCC: $22.00 © 2002 American Chemical Society
Published on Web 08/03/2002

general agreement on the dominant benzene formation pathway.[12] In particular, while extensive, but not conclusive, work has been carried out on the benzene formation from linear molecule cyclization, until now relatively less effort has been devoted to investigate the cyclopentadiene production channels and its successive reactions to benzene.

For instance, Westmoreland et al.[12] carried out a systematic screening of benzene formation pathways using the idea of chemical activation (chemically activated intermediates can form aromatics directly from the reactants without producing any observable intermediate) and the quantum Rice−Ramsperger−Kassel (QRRK) approach. However, they have not considered the cyclopentadiene channels, and several reaction rates used for the QRRK computations have been estimated using thermochemical kinetics or other simplified methods.

In this framework, the main aim of this work has been to investigate the cyclopentadiene production pathway from vinyl radical and 1,3-butadiene. Because of the lack of experimental information and to allow a fair comparison among different reaction channels, all of the relevant thermodynamic and kinetic parameters required by the QRRK approach have been estimated through quantum chemistry methods. Moreover, with the aim of validating the proposed approach, a comparison with some experimental results concerning similar reactions has been carried out and other chemical reactions relevant for cyclo hydrocarbons with five and six carbon atoms have been also investigated.

2. Method

The reaction between C_2H_3 and C_4H_6 is a complex process that, depending on the operating conditions, can yield a variety of products. To investigate the relative importance of the different reaction paths, as well as to determine the absolute rate of addition of C_2H_3 and C_4H_6, we used quantum Rice−Ramsperger−Kassel (QRRK) theory, as modified by Dean[13] to extend it to bimolecular reactions. The parameters needed by QRRK are the rate of intermolecular energy transfer between excited and nonexcited species, the kinetic constants for each elementary reaction, and the mean vibrational frequencies for all of the reacting chemical species. Because many of these parameters are not known for the reacting species here considered, they were calculated from first principles. Quantum chemistry, because of the development of high-accuracy methods and the increase of computer speed, is in fact being used more and more to determine reaction pathways and kinetic constants relevant to PAH and soot formation.[14,15] The rate of intermolecular energy transfer was evaluated as suggested by Troe[16] adopting Lennard-Jones collision rates with collisional efficiencies, β, calculated as follows:

$$\frac{\beta}{1-\beta^{0.5}} = \frac{-\Delta E}{1.15 k_b T} \tag{9}$$

where ΔE is the mean energy transferred per collision, for which a −980 cal/mol value was adopted. This is consistent with a N_2 collision partner, the species present in the highest concentration when the combustion environment is air.

Forward kinetic constants for all of the elementary reactions involved in the reaction mechanism were calculated with quantum chemistry. Backward kinetic constants were determined from the forward kinetic constants by applying thermodynamic consistence (i.e., using the equilibrium constant) with calculated entropy and enthalpy changes. Geometries of reactants, products, and transition states were optimized adopting density functional

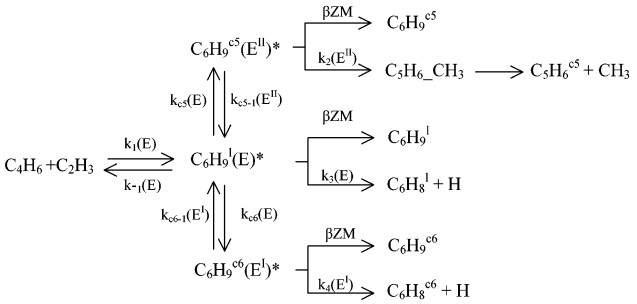

Figure 1. Kinetic pathway following the reaction of addition of C_2H_3 to C_4H_6.

theory, with correlation and exchange energies calculated with the B3LYP functionals[17] and the 6-31G(d,p) basis set. The stability of all of the optimized structures was characterized through frequency calculations. A structure was considered stable only if it was without imaginary frequencies, and transition states were characterized by a single imaginary frequency. The energy of each molecule was calculated using a procedure similar to that adopted in the G2MP2 method.[18] The energy of the molecule, the structure of which was determined with the B3LYP/6-31G(d,p) method, was first calculated at the QCISD(T)/6-311+G(d,p) level. A correction for the basis set error was determined by subtracting from the energy calculated with the MP2 method with the 6-311++G-(3dp,2f) that calculated with the 6-311+G(d,p) basis set. Then, energies were corrected for remaining deficiencies (higher-level correction, HLC) adopting the empirical factors determined by Curtiss et al.[18] for each α and β valence electron for the G2MP2 method (4.8 and 0.19 mhartree, respectively). The thermal contribution (TE) to energy at 300 K, including zero-point energy (ZPE), calculated with B3LYP/6-31(g,p) was finally added, resulting in the following expression for the energy:

$$E = E(\text{QCISD(T)/6-311G(d,p)}) + E(\text{MP2/6-311++G(3dp,2f)}) - E(\text{MP2/6-311G(3d,p)}) + \text{HLC} + \text{ZPE} + \text{TE} \tag{10}$$

This method differs from the standard G2MP2 theory in that the structures were optimized with B3LYP rather than MP2. This modification is similar to that used in the G3 method[19] and increased the accuracy of the calculated energies. Finally, kinetic constants of each reaction were corrected for the tunneling effect adopting the Wigner's perturbation theory equation.[20] All calculations were performed with the Gaussian 98 suite of programs.[21] Low vibration frequencies (i.e., smaller than 100 cm^{-1}) in transition states were explicitly treated as rotors following the rules suggested by Gilbert et al. for unimolecular reactions.[22]

In the following, we distinguish kinetic constants calculated with QRRK theory, which are the result of a complex reaction mechanism, from those of elementary reactions, calculated with transition-state theory (TST), referring to them as QRRK and TST rate coefficients, respectively.

3. Results and Discussion

3.1. Evaluation of TST Rate Coefficients. The overall reaction scheme considered is reported in Figure 1. The reaction is started by the addition of C_2H_3 to C_4H_6 to form the linear hexadienyl radical ($C_6H_9^l$). Because the reaction is exothermic, $C_6H_9^l$ is in a vibrationally excited state ($C_6H_9^{l*}$). Five different reactions are then possible. The first is the deactivation due to the collision with the bath gas resulting in the formation of

TABLE 1: Calculated TST Rate Coefficients, $k = AT^{\alpha} \exp(-E/(RT))$[a]

	reaction	A_{forw}	α	$E_{a,forw}$	A_{back}	α	$E_{a,back}$
k_1	$C_2H_3 + C_4H_6 \rightarrow C_6H_9^{l}$	4.2×10^{13}	0	2.8	1.0×10^{20}	−1.0	48.7
k_{c5}	$C_6H_9^{l} \rightarrow C_6H_9^{c5}$	6.4×10^{11}	0	21.2	8.32×10^{12}	0	22.2
k_{c6}	$C_6H_9^{1} \rightarrow C_6H_9^{c6}$	1.1×10^{12}	0	23.2	8.7×10^{13}	0	30.1
k_2	$C_6H_9^{c5} \rightarrow C_5H_6{-}CH_3$	1.4×10^{13}	0	30.0	4.1×10^{13}	0	48.3
k_3	$C_6H_9^{1} \rightarrow C_6H_8^{l} + H$	6.3×10^{12}	0	40.0	1.8×10^{10}	1	2.0
k_4	$C_6H_9^{c6} \rightarrow C_6H_8^{c6} + H$	1.7×10^{13}	0	32.5	8.8×10^{9}	1	1.3
k_5	$C_5H_6{-}CH_3 \rightarrow C_5H_6 + CH_3$	2.0×10^{13}	0	39.4	2.8×10^{7}	1	6.8

[a] Geometries were optimized with B3LYP/6-31G(d,p); frequencies were calculated with B3LYP/6-31G(d,p); energies were calculated with G2MP2, modified as described in the text, on geometries optimized with B3LYP/6-31G(d,p). Preexponential factor and activation energies are reported in units consistent with kcal, s, mol, and cm. The rate coefficients of the backward reactions were calculated through the thermodynamic consistence with calculated free energy changes.

$C_6H_9^{l}$. Alternatively, $C_6H_9^{l}$* can cyclize forming two species: the cyclopentendienyl radical ($C_6H_9^{c5}$) or the cyclohexenyl radical ($C_6H_9^{c6}$). Finally, $C_6H_9^{l}$* can dissociate into the reactants or lose a hydrogen atom and form $C_6H_8^{l}$. Both $C_6H_9^{c5}$ and $C_6H_9^{c6}$, produced by cyclization of $C_6H_9^{l}$*, are in an excited state, with an energy equal to that of the excited state of $C_6H_9^{l}$* from which they are produced plus the reaction energy change. The reactivity of the two excited species is similar to that of $C_6H_9^{l}$*: they can either dissociate to $C_5H_6^{c5}$ and $C_6H_8^{c6}$ or open the aromatic ring and form again $C_6H_9^{l}$* or collide with a molecule of the bath gas and give the corresponding nonexcited species. The dissociation of $C_6H_9^{c5}$ into $C_5H_6^{c5}$ and CH_3 proceeds through the formation of the methylcyclopentenyl radical ($C_5H_6{-}CH_3$). Because the activation energy for $C_5H_6{-}CH_3$ to give back $C_6H_9^{c5}$ is higher than that required to dissociate into $C_5H_6^{c5}$ and CH_3 (48.3 vs 30.0 kcal/mol), we assumed that the reaction from $C_6H_9^{c5}$ to $C_5H_6^{c5}$ and CH_3 occurs in a single reactive step. The TST rate coefficient was set equal to that of the conversion of $C_6H_9^{c5}$ into $C_5H_6{-}CH_3$. The kinetic constant of the reaction of addition of $C_6H_8^{c6}$ and H has been experimentally measured[23] at 298 K and is in good agreement with the calculated value (9.0×10^{11} vs 3.0×10^{11} cm^3/(mol s)).

The formulation of QRRK theory that we used is reported by Dean[13] for reactions with two possible excited species. Here, the equations were modified to account for three parallel reaction paths. The rate equations can be derived straightforwardly by applying the steady-state condition to the excited molecules $C_6H_9^{l}$*, $C_6H_9^{c5}$*, and $C_6H_9^{c6}$*. In this procedure, it is important to calculate the quantized thermal energy distribution, $k(E,T)$, from the bottom of the potential well for each excited species. In particular, the potential well of $C_6H_9^{c5}$* and $C_6H_9^{c6}$* differs from that of $C_6H_9^{l}$* by a value equal to the difference between the respective enthalpies of formation. Kinetic constants of all considered reactions were determined through the conventional transition-state theory and the calculated preexponential factors and activation energies are reported in Table 1. The tunneling correction was significant for the reaction from $C_6H_9^{c5}$ to $C_5H_6{-}CH_3$, for which an imaginary vibrational frequency of 2078 cm^{-1} was calculated. The transition-state structures for the C_2H_3 and C_4H_6 addition reaction, for the two cyclization reactions, and for the formation of the $C_5H_6^{c5}$ species are reported in Figure 2. All of the calculated transition states were without low vibrational frequencies except for the reaction between C_2H_3 and C_4H_6.

The rate of the reaction of addition of C_2H_3 to C_4H_6 influences the overall rate of the process. The calculated activation energy is 2.8 kcal/mol and the preexponential factor, determined through conventional transition-state theory with vibrational frequencies and moments of inertia calculated from the optimized structure, is 1.05×10^{11} cm^3/(mol s). The transition state of this reaction presents five low vibrational frequencies: 27.4, 55.5, 120.9, 131.7, and 173.4 cm^{-1}. In the harmonic oscillator approximation, a small vibrational frequency can be indicative of a small energetic barrier for the relative motion of a part of the molecule with respect to the other. This suggests that some of the lowest vibrational degrees of freedom might be best treated as rotors rather than vibrations. For this reason, the rotational motions corresponding to each vibration were analyzed in detail. The first two low vibrational frequencies can be attributed to the bending of the C_2H_3 fragment with respect to the $C_2H_3{-}C_4H_6$ bond (as sketched in Figure 3, first and second rocking motion), while the last two correspond to the bending of C_4H_6 with respect to the same bond. The 120.9 cm^{-1} vibrational frequency is the torsional motion around the $C_2H_3{-}C_4H_6$ bond, and in the lack of detailed information on the potential energy surface for this motion, it was treated as a vibration. It can be observed that, if this motion were treated as an unhindered rotation, the rotational partition function value would be 4.8 at 300 K, with respect to the 2.3 value of the corresponding vibrational partition function. Because 4.8 can be considered as the upper limit of the partition function of the torsional motion and even a small energy barrier for the rotation would rapidly decrease its value to the vibrational limit, it can be concluded that the error introduced with this approximation is negligible. For each of the four remaining vibrations, a few points were taken on the potential energy surface of the corresponding rotation. It was found that a large energy barrier prohibits the rocking motion on the C1−C2−C3 plane (see Figure 3), which corresponds to the 55.5 and 173.4 cm^{-1} vibrational frequencies, while the other motion is almost unhindered. The energy barrier preventing the first rocking motion is probably due to the repulsive interaction of the hydrogen atom (labeled H1 in Figure 3) of the C_2H_3 fragment with C_4H_6. Accordingly, the first motion was treated as a vibration, while the second was considered as a free rotor. Because each internal motion corresponds to two vibrational frequencies, the TST rate coefficient was calculated considering two vibrational modes (27.4 and 131.7 cm^{-1}) as internal rotations. The value so calculated is 4.2×10^{13} cm^3/(mol s), thus significantly larger than that calculated with conventional transition-state theory considering all internal motions as vibrations (1.05×10^{11} cm^3/(mol s)).

In Tables 2 and 3, enthalpy changes and activation energies for the considered reactions determined at different levels of theory are reported. The modified G2MP2 theory calculates reaction enthalpies that differ from the available experimental values by a mean value of 0.9 kcal/mol. The error is larger for the B3LYP results, with a mean difference between calculated and experimental data equal to 2.7 kcal/mol. Curtiss et al.[18] calculated the mean absolute deviation from experimental values for the G3X(MP2) theory, which is essentially similar to the method here adopted, to be 1.19 kcal/mol. With this value, the

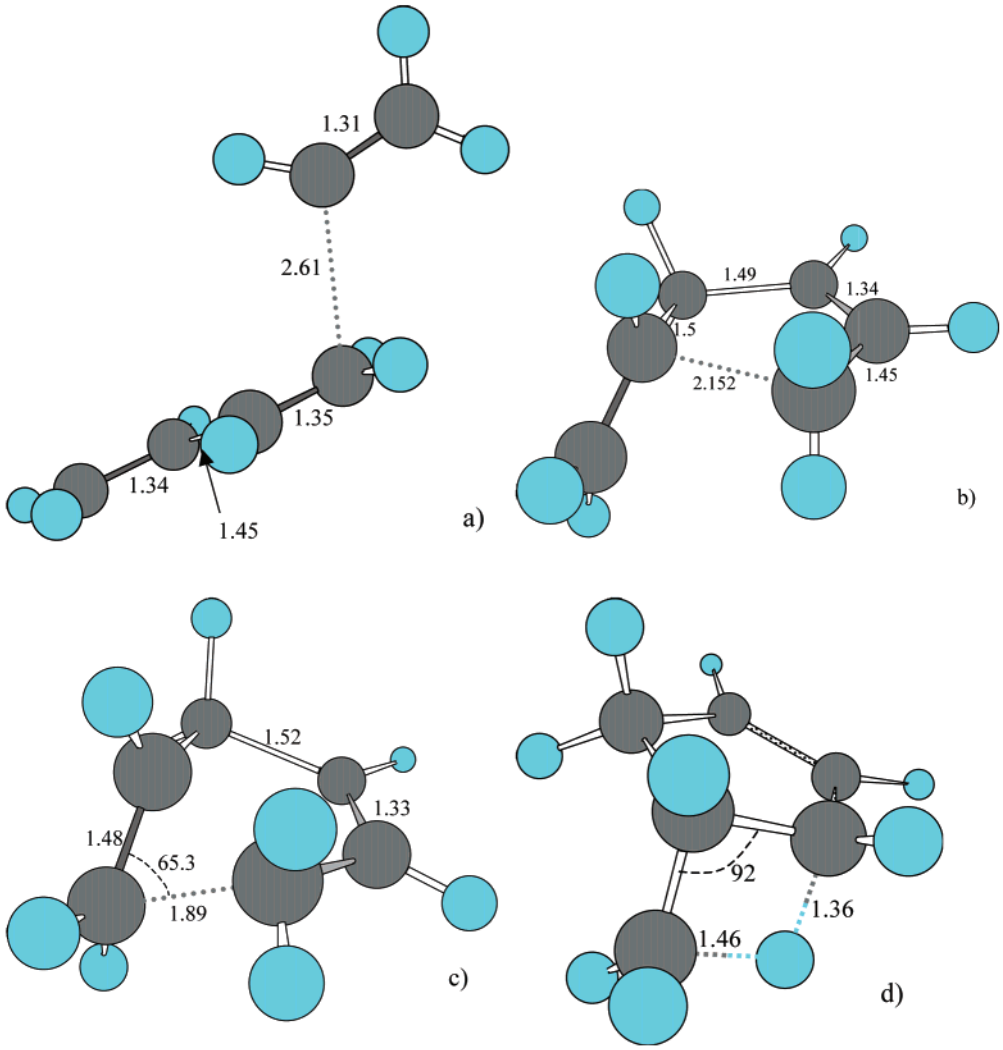

Figure 2. Transition state structure for the reactions (a) $C_2H_3 + C_4H_6 \rightarrow C_6H_9^1$, (b) $C_6H_9^1 \rightarrow C_6H_9^{c5}$, (c) $C_6H_9^1 \rightarrow C_6H_9^{c6}$, and (d) $C_5H_6^{c5} \rightarrow C_5H_6^{c5}-CH_3$. Distances are reported in Å and angles in deg.

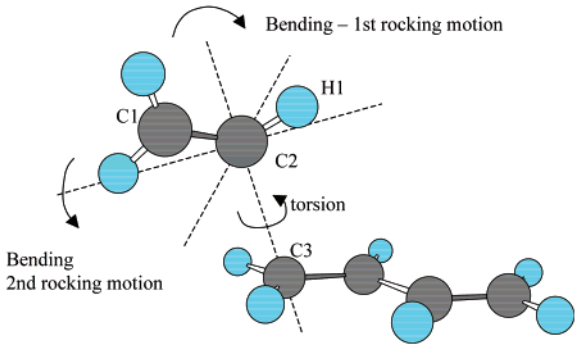

Figure 3. Rotational motion of the C_2H_3 radical in the $C_2H_3 + C_4H_6$ reaction.

average error at 1000 K for the calculation of TST rate coefficient in the Arrhenius form is smaller than 2, which is often within the experimental uncertainties for kinetic constants measurements. It can be also observed that the modified G2MP2 method offers a substantial improvement over the activation energies calculated with the B3LYP method. This result is obtained performing only two single-point energy calculations (QCISD(T) and MP2/6-311++(3dp,2f)) after optimizing the reactants and transition-state structures with B3LYP.

3.2. Validation through Comparison with $C_2H_3 + C_3H_6$ Reaction Data. A detailed study of the reaction of addition of C_2H_3 and C_4H_6 would require the complete mapping of the potential energy surface for the different rotational motions. Then, the corresponding partition functions should be evaluated, thus explicitly treating the low vibrational frequencies as rotors hindered by an energy barrier (e.g., Speybroek et al.[24]). Unfortunately, the numerical calculation of the potential energy surface requires optimizing the transition-state structure at different rotational angles for a large number of points, which is extremely computationally demanding at the level of theory here adopted. Thus, because the error associated with the simplified treatment of the internal rotational degrees of freedom is not easily estimated, we used the same approach to determine the rate constant for the reaction between C_2H_3 and C_3H_6. This process is similar to the one that we are investigating, and it has been experimentally studied.[25] Kinetic constants for the two major reaction pathways were measured with an uncertainty factor of 3. The transition state for the reaction of addition of C_2H_3 and C_3H_6, shown in Figure 4, is geometrically similar to that of the former reaction, and it is characterized by five low vibrational frequencies: 11, 97, 132, 165, and 217 cm^{-1}. They correspond to the same rocking and torsional motions found for the reaction of addition of C_2H_3 and C_4H_6 and were therefore treated as two 1-dimensional free rotors and three vibrations. The preexponential factor calculated is equal to 9.9×10^{11} cm^3/(mol s), while the activation energy is equal to 4.4 kcal/mol.

TABLE 2: Comparison among Reaction Enthalpy Changes (kcal/mol) Calculated at 298 K and 1 Atm with Different Quantum Chemistry Methods[a]

	B3LYP/ 6-31G(d,p)	QCISD(T)/ 6-311+G(d,p)	MP2/ 6-311+G(3df,2p)	MP2/ 6-311+G(d,p)	G2MP2*	expt[30]
$C_2H_3 + C_4H_6 \rightarrow C_6H_9^l$	−45.4	−50.7	−53.9	−53.2	−45.1	
$C_6H_9^l \rightarrow C_6H_9^{c5}$	1.1	−3.8	−8.8	−12.5	0	
$C_6H_9^l \rightarrow C_6H_9^{c6}$	−6.2	−8.8	−14.4	−16.3	−6.9	
$C_6H_9^{c5} \rightarrow C_5H_6^{c5} + CH_3$	14.6	17.3	14.2	16.7	14.9	
$C_6H_9^l \rightarrow C_6H_g^l + H$	40.4	38.6	28.0	28.6	38.0	
$C_6H_9^{c6} \rightarrow C_6H_g^{c6} + H$	35.3	31.7	26.1	27.3	30.4	
$C_2H_3 + C_4H_6 \rightarrow C_5H_6^{c5} + CH_3$	−31.7	−30.4	−41.7	−42.5	−29.5	−29.0
$C_2H_3 + C_4H_6 \rightarrow C_6H_8^{c6} + H$	−17.8	−20.3	−34.8	−34.8	−20.4	−20.9
$C_2H_3 + C_4H_6 \rightarrow C_6H_8^l + H$	−7.1	−5.2	−19.0	−17.8	−6.4	−4.8

[a] G2MP2* is different from the original G2MP2 method in that geometries were optimized with B3LYP/6-31G(d,p). All energies are corrected for ZPE and thermal energies with frequencies calculated with B3LYP/6-31G(d,p).

TABLE 3: Comparison among Activation Energies Calculated with Different Quantum Chemistry Methods[a]

	B3LYP/ 6-31G(d,p)	QCISD(T)/ 6-311+G(d,p)	MP2/ 6-311+G(3df,3p)	MP2/ 6-311+G(d,p)	G2MP2*
$C_6H_3 + C_4H_6 \rightarrow C_6H_9^l$	1.3	3.1	15.5	15.7	2.8
$C_6H_9^l \rightarrow C_6H_9^{c5}$	17.9	20.7	24.5	23.8	21.3
$C_6H_9^l \rightarrow C_6H_g^{c6}$	22.5	22.6	30.1	29.5	23.2
$C_6H_9^{c5} \rightarrow C_5H_6^{c5} + CH_3$	30.2	32.6	40.2	39.5	30.1
$C_6H_9^l \rightarrow C_6H_g^l + H$	41.3	41.4	32.0	33.2	40.2
$C_6H_9^{c6} \rightarrow C_6H_g^{c6} + H$	36.0	35.1	34.5	37.0	32.6

[a] The G2MP2* method is different from the original G2MP2 method in that geometries were optimized with B3LYP/6-31G(d,p).

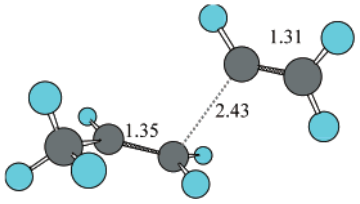

Figure 4. Transition-state structure for the reaction of addition of C_2H_3 and C_3H_6.

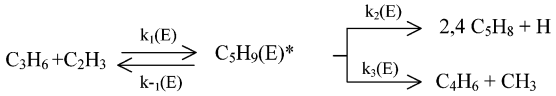

Figure 5. Kinetic pathway following the reaction of addition of C_2H_3 and C_3H_6.

TABLE 4: Calculated TST Rate Coefficients of the Elementary Processes Involved in the Reaction of Addition of C_2H_3 and C_3H_6[a]

	reaction	A_{forw}	$E_{a,forw}$	A_{back}	α	$E_{a,back}$
k_1	$C_2H_3 + C_3H_6 \rightarrow C_5H_9$	3.4×10^{12}	4.4	3.2×10^{18}	−1	44
k_2	$C_5H_9 \rightarrow 2,4\text{-}C_5H_8 + H$	2.2×10^{12}	35.1			
k_3	$C_5H_9 \rightarrow C_4H_6 + CH_3$	5.5×10^{12}	32.0			

[a] Geometries were optimized with B3LYP/6-31G(d,p); frequencies were calculated with B3LYP/6-31G(d,p); energies were calculated with G2MP2 on geometries optimized with B3LYP/6-31G(d,p). Preexponential factor and activation energies are reported in units consistent with kcal, s, mol, and cm.

The QRRK preexponential coefficient calculated considering all internal motions as vibrations is 7.3×10^{10} cm^3/(mol s). The possible products of the reaction through the reaction paths shown in Figure 5 are C_4H_6 and C_5H_8. TST rate coefficients for the reactions from C_5H_9 to C_4H_6 and C_5H_8 were calculated as well and are reported in Table 4.

QRRK theory was used to evaluate the overall reaction rate for the formation of the reaction products from C_2H_3 and C_3H_6. The mean vibrational frequency of the activated complex calculated through quantum chemistry was equal to 1051.1 cm^{-1}, while the Lennard-Jones parameters for C_5H_9 were calculated adopting the Fuller contribution volumes method[26] as 5.9 Å and 178.7 K. The collision partner was N_2, and all of the calculations were performed at atmospheric pressure. The comparison between calculated and experimental rate coefficients is reported in Figure 6. The experimental values are overestimated by a factor of 3 at 500 K, are almost equal to the calculated values at 1000 K, and are underestimated at 1500 K by a factor of 4, which is similar to the experimental uncertainty. The decrease of reaction rates at higher temperatures is determined by the increase of the reaction rate of the backward reaction, which decreases the concentration of the excited species C_5H_9*. This trend, which is not confirmed experimen-

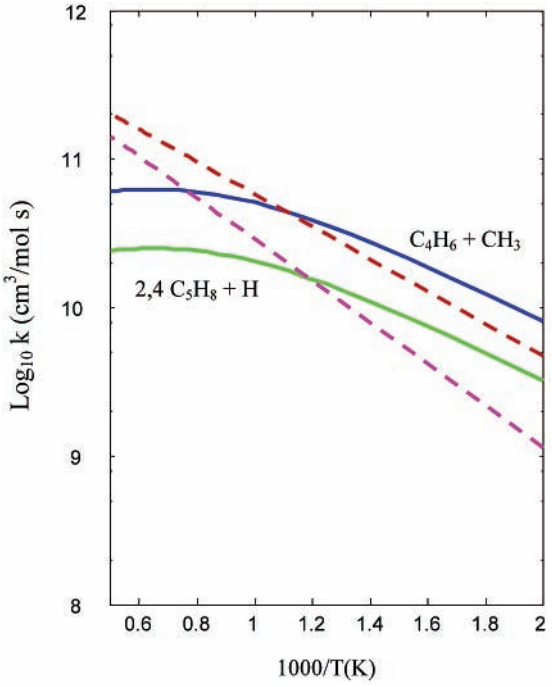

Figure 6. Comparison between experimental (− − −) and calculated (—) QRRK rate coefficients at 1 atm for the reaction of formation of 2,4-C_5H_8 + H and C_4H_6 + CH_3 from C_2H_3 and C_3H_6.

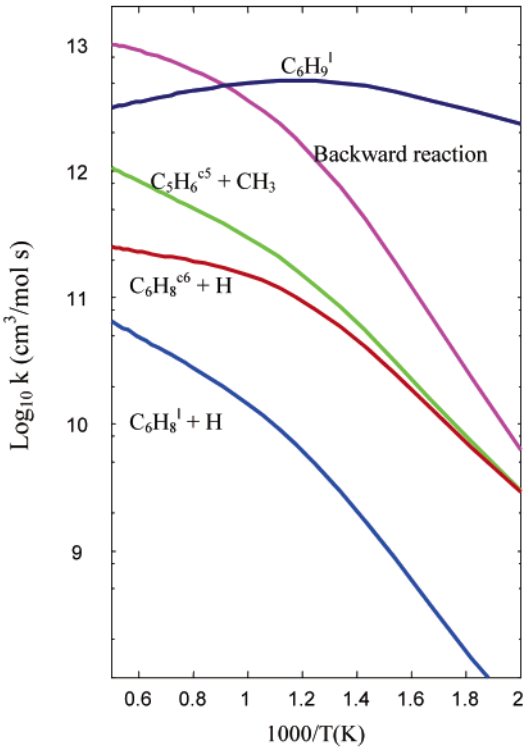

Figure 7. QRRK rate coefficients calculated for the addition of C_2H_3 to C_4H_6 at 1 atm. All possible products were considered. Backward reaction refers to $C_6H_9^{l} \rightarrow C_2H_3 + C_4H_6$.

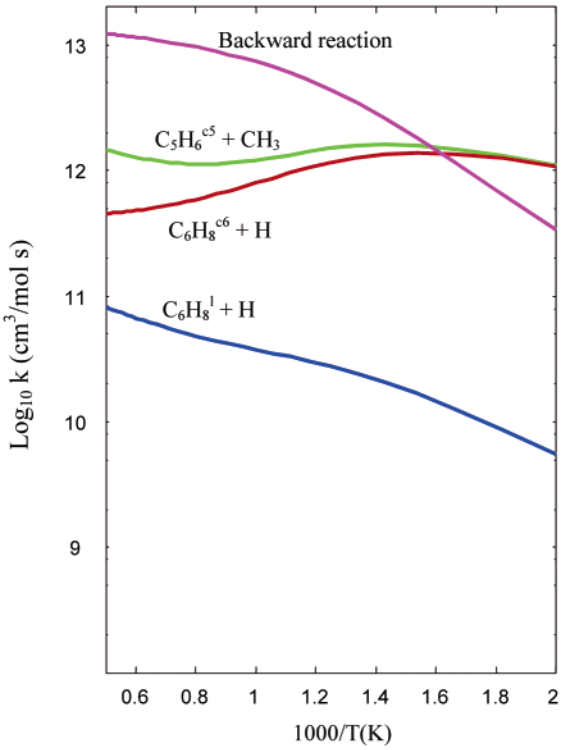

Figure 8. QRRK rate coefficients calculated for the addition of C_2H_3 and C_4H_6 at 1 atm. The net rate of formation of adducts ($C_6H_9^{l}$, $C_6H_9^{c5}$, and $C_6H_9^{c6}$) was set equal to 0. Backward reaction refers to $C_6H_9^{l} \rightarrow C_2H_3 + C_4H_6$.

tally, might be caused by the simplified treatment of the vibrational degrees of freedom made by QRRK theory, which assumes all of the molecular vibrations to be equal to the mean molecular vibrational frequency. The ratio between the rates of formation of the two products is also similar to that experimentally determined. These results were obtained assuming that C_5H_9 is not formed as a stable product of the reaction. In other words, when formed from collisional stabilization of C_5H_9*, it rapidly reacts with a bath molecule to give back the excited state.

3.3. Analysis of the $C_2H_3 + C_4H_6$ Reaction. The same approach successfully used to investigate the addition of C_2H_3 and C_3H_6 was then applied to study the more complex reaction of addition of C_2H_3 to C_4H_6. Lennard-Jones parameters for the collisional stabilization reaction were found in the literature.[12] The mean vibrational frequencies of the excited molecules were evaluated with calculated vibrational frequencies and were 990, 1062, and 1129 cm^{-1} for $C_6H_9^{l}$*, $C_6H_9^{c5}$*, and $C_6H_9^{c6}$*, respectively. The QRRK rate coefficients for the reactions of production of $C_5H_6^{c5}$, $C_6H_8^{c6}$, $C_6H_8^{l}$, and $C_6H_9^{l}$, calculated at 1 atm as a function of temperature, are shown in Figure 7. The QRRK rate coefficient for the backward reaction, that is, the reaction from excited $C_6H_9^{l}$* back to C_2H_3 and C_4H_6, is also reported for comparison. As its rate increases, the rates of all of the overall reactions from the reactants to the various products correspondingly decrease. The species produced in the largest amount is $C_6H_9^{l}$, followed by $C_5H_6^{c5}$, $C_6H_8^{c6}$, and $C_6H_8^{l}$. The higher rate of production of $C_5H_6^{c5}$ with respect to $C_6H_8^{c6}$ comes from a kinetic effect. In fact, the $C_6H_9^{c5}$* adduct is thermodynamically less stable by 6.5 kcal/mol than $C_6H_9^{c6}$*. Therefore, even if the activation energy for the formation of $C_6H_9^{c5}$* is smaller than that for the formation of $C_6H_9^{c6}$*, the backward reaction is faster. This results in a lower concentration of the $C_6H_9^{c5}$* excited species with respect to $C_6H_9^{c6}$*. The rate of production of $C_5H_6^{c5}$ is higher anyway because the TST rate coefficient for its formation from $C_6H_9^{c5}$* is faster than that for the formation of $C_6H_8^{c6}$ from $C_6H_9^{c6}$*. From the analysis of the data reported in Figure 7, it appears evident that the temperature dependence of many of the considered reactions is markedly non-Arrhenius. This is a consequence of the explicit consideration of the population of the excited states of the intermediates, which are formed as a step of the reactive process, as well as of the complexity of the reaction mechanism.

The products formed through collisional stabilization, $C_6H_9^{l}$, $C_6H_9^{c5}$, and $C_6H_9^{c6}$, are thermodynamically unstable at high temperatures and are therefore likely to react rapidly once formed. In a combustion environment in which N_2 is the most abundant species, it is reasonable to assume that, after being generated, they get back to their excited state through collisional excitation. This assumption is reproduced imposing a zero net production rate for these species. Performing the calculations under this hypothesis, the results reported in Figure 8 are obtained. The species produced at the highest rate is now $C_5H_6^{c5}$, with an increase of the QRRK rate coefficient with respect to the case when the formation of the stabilized adducts was considered equal to a factor of 5 at 1000 K. The same effect is observed for $C_6H_8^{c6}$ formation reactions. The Arrhenius parameters of the QRRK rate coefficients for the formation of $C_5H_6^{c5}$, $C_6H_8^{c6}$, $C_6H_8^{l}$, $C_6H_9^{l}$, $C_6H_9^{c5}$, and $C_6H_9^{c6}$ were fitted through nonlinear regression both for when the formation of collisional stabilized adducts was neglected and for when it was not neglected, and they are reported in Table 5. The QRRK rate coefficients were interpolated at two different pressures (1 and 0.01 atm). It can be observed that neglecting the collisional stabilization pathways makes the reactions pressure-independent. A comparison between the QRRK rate coefficients calculated with the full kinetic scheme of Figure 1 and without collisional stabilization is reported in Figure 9 as a function of pressure at 1000 K. As expected, when the pressure is reduced, the QRRK rate coefficient approaches asymptotically the pressure-inde-

TABLE 5: QRRK Rate Coefficients for the Reaction of Addition of C_2H_3 and C_4H_6[a]

reaction	$P = 1$ atm			$P = 0.01$ atm.		
	$\log_{10} A$	α	E_a	$\log_{10} A$	α	E_a
	Products $C_5H_6^{c5}$, $C_6H_8^{c6}$, $C_6H_8^{l}$					
$C_2H_3 + C_4H_6 \rightarrow C_5H_6^{5} + CH_3$	30.4	−5.73	6247	30.4	−5.73	6247
$C_2H_3 + C_4H_6 \rightarrow C_6H_8^{c6} + H$	31.6	−6.19	6036	31.6	−6.19	6036
$C_2H_3 + C_4H_6 \rightarrow C_6H_8^{l} + H$	19.1	−2.42	6053	19.1	−2.42	6053
	Products $C_5H_6^{c5}$, $C_6H_8^{c6}$, $C_6H_8^{l}$, $C_6H_9^{c6}$, $C_6H_9^{c5}$					
$C_2H_3 + C_4H_6 \rightarrow C_5H_6^{5} + CH_3$	28.4	−5.08	7141	30.5	−5.73	7097
$C_2H_3 + C_4H_6 \rightarrow C_6H_8^{c6} + H$	32.1	−6.19	8130	33.7	−6.71	7733
$C_2H_3 + C_4H_6 \rightarrow C_6H_8^{l} + H$	17.9	−2.06	6050	18.0	−2.14	5396
$C_2H_3 + C_4H_6 \rightarrow C_6H_9^{c6}$	31.0	−6.54	1835	44.8	−11.22	6903
$C_2H_3 + C_4H_6 \rightarrow C_6H_9^{c5}$	66.7	−16.76	21 037	57.6	−14.90	12 714
	Products $C_5H_6^{c5}$, $C_6H_8^{c6}$, $C_6H_8^{l}$, $C_6H_9^{c6}$, $C_6H_9^{c5}$, $C_6H_9^{l}$					
$C_2H_3 + C_4H_6 \rightarrow C_5H_6^{5} + CH_3$	33.3	−6.18	16 065	23.6	−3.62	4685
$C_2H_3 + C_4H_6 \rightarrow C_6H_8^{c6} + H$	35.6	−6.98	16 462	26.7	−4.65	5537
$C_2H_3 + C_4H_6 \rightarrow C_6H_8^{l} + H$	27.8	−4.65	17 116	17.8	−1.99	6810
$C_2H_3 + C_4H_6 \rightarrow C_6H_9^{c6}$	−2.48	3.76	−7894	−32.2	12.16	−24 588
$C_2H_3 + C_4H_6 \rightarrow C_6H_9^{c5}$	46.8	−10.79	15 068	39.4	−9.45	5158
$C_2H_3 + C_4H_6 \rightarrow C_6H_9^{l}$	45.7	−10.16	13 223	40.3	−9.36	5185

[a] Three cases involving different products were considered. The kinetic constant values were fitted between 500 and 2500 K at 1 and 0.01 atm. $k = AT^{\alpha} \exp(-E_a/(RT))$. Preexponential factor and activation energies are reported in units consistent with kcal, s, mol, and cm.

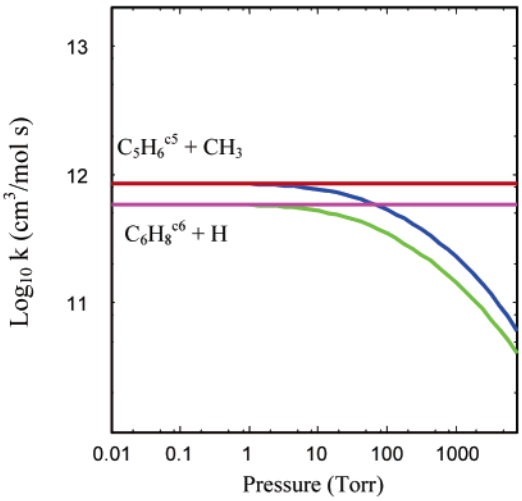

Figure 9. Comparison between the QRRK rate coefficients calculated for the reaction of addition of C_2H_3 to C_4H_6 toward $C_5H_6^{c5}$ and $C_6H_8^{c6}$ at 1000 K both considering and neglecting the formation of stabilized adducts.

pendent value. It is interesting to analyze the relative importance of the different reaction channels analyzed. If we consider the C_6H_9 adducts as stable species, at 1000 K and 1 atm the relative rate of formation of $C_5H_6^{c5}$, $C_6H_8^{l}$, $C_6H_9^{l}$, $C_6H_9^{c5}$, and $C_6H_9^{c6}$ with respect to $C_6H_8^{c6}$ is 1.6, 0.11, 18.3, 1.2, and 0.3, respectively. If we neglect the formation of stabilized adducts, then the relative rate of formation of $C_5H_6^{c5}$, $C_6H_8^{l}$, and $C_6H_8^{c6}$ in the same conditions becomes 1.45, 0.06, and 1.

It is also important to note that the QRRK rate coefficients for the reaction of addition of C_2H_3 to C_4H_6 can account for the formation of benzene in butadiene flames at low pressure (2.67 kPa) and a fuel equivalence ratio of 2.4. The rate of formation of benzene experimentally measured[27] ranges from about 5×10^{-8} to 8×10^{-7} mol/(cm^3 s). In the same conditions, the rates of formation of $C_5H_6^{c5}$ and $C_6H_8^{c6}$ determined using the QRRK rate coefficients, the measured concentrations of C_2H_3 and C_4H_6, and the measured temperature range from 2×10^{-7} to 9×10^{-7} and from 9×10^{-8} to 6×10^{-7} mol/(cm^3 s), respectively.

The same conclusions arise also from the comparison with the concentrations of $C_6H_8^{c6}$ and $C_5H_6^{c5}$ measured by Brezinsky et al.[29] in butadiene flames at atmospheric pressure and for fuel equivalence ratios varying between 0.55 and 1.65. According to the reaction mechanism here proposed, $C_6H_8^{c6}$ and $C_5H_6^{c5}$ are formed at a similar rate, with $C_5H_6^{c5}$ being slightly more abundant than $C_6H_8^{c6}$. This is in agreement with the experimental results in a wide range of fuel equivalence ratio values.

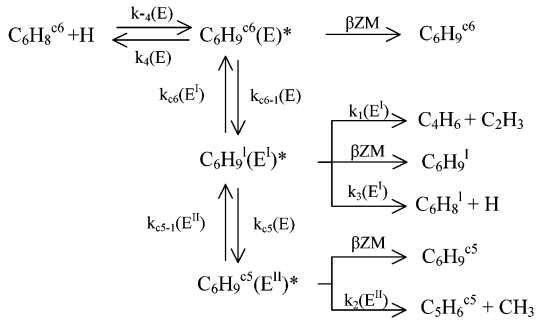

Figure 10. Kinetic pathway considered for the reaction of addition of $C_6H_8^{c6}$ and H.

3.4. Analysis of the $C_6H_8^{c6}$ + H and $C_5H_6^{c5}$ + CH_3 Reactions. These reactions, which follow backward the same reaction pathway previously described, are important because they can influence the net rate of production of *cyclo*-C_5 and -C_6 species. The reaction rates previously estimated for the kinetic scheme reported in Figure 1 allow for a fast computation of the necessary kinetic parameters.

First, the addition of hydrogen to cyclohexadiene, which follows the mechanism reported in Figure 10, was investigated. The reaction proceeds through the formation of the $C_6H_9^{c6}$* adduct, which can then be stabilized through collision with the bath gas or can open the cyclic hydrocarbon forming $C_6H_9^{l}$*. The linear C_6 adduct can then decompose into C_2H_3 and C_4H_6; $C_6H_8^{l}$ and H, be stabilized through collision with the bath gas or form the $C_6H_9^{c5}$* adduct. It can be argued that the direct pathway leading from $C_6H_9^{c6}$* to $C_6H_9^{c5}$* might be faster than passing from the intermediate $C_6H_9^{l}$* species. This reaction was investigated, and its transition-state was determined. The activation energy, calculated at the B3LYP/6-31G(d,p) level, is equal to 61 kcal/mol, significantly higher than the 23 kcal/mol necessary to form $C_6H_9^{l}$*. Accordingly, it appeared reasonable to neglect this reaction pathway. We can see that, apart from k_{-4}, all of the other kinetic parameters involved in the

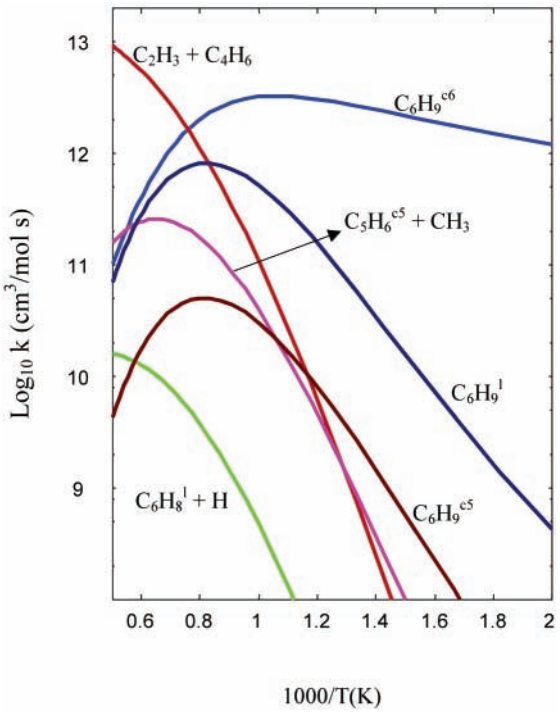

Figure 11. QRRK rate coefficients calculated for the addition of $C_6H_8^{c6}$ and H at 1 atm. All possible products were considered.

reaction scheme have been already estimated in the previous part of this work. This allows, at the expense of a single reaction rate estimation, us to compute the kinetic parameters for all of the paths reported in Figure 10. The results of the calculations carried out using the parameters reported in Table 1 are shown in Figure 11. $C_6H_9^{c6}$, followed by $C_6H_9^{l}$ and $C_6H_9^{c5}$, is the principal product of the reaction at low temperatures, while C_2H_3 and C_4H_6 are the most rapidly produced species at higher temperatures. Neglecting the formation of all of the stabilized adducts, similarly to what was done for the addition of C_2H_3 and C_4H_6, determines an increase of the net rate of formation of C_4H_6 and C_2H_3, $C_5H_6^{c5}$ and CH_3, and $C_6H_8^{l}$ and H. QRRK rate coefficients for the various reaction channels, interpolated between 500 and 2500 K, are reported in Table 6 at 1 and 0.01 atm. Three different cases were considered. In the first, all of the species were explicitly considered as possible products of the reaction; in the second, the QRRK rate coefficients were computed assuming that the net rate of production of $C_6H_9^{l}$ is negligible; in the third, the formation of $C_6H_9^{c6}$ and $C_6H_9^{c5}$ was also neglected.

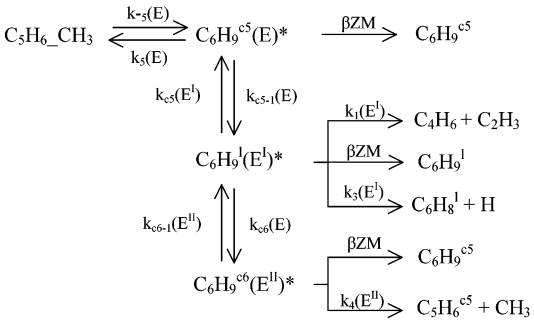

Figure 12. Kinetic pathway considered for the reaction of decomposition of $C_5H_6-CH_3$.

In a similar way, the reaction between $C_5H_6^{c5}$ and CH_3 has also been investigated. This reaction proceeds in two steps. First, methyl reacts with $C_5H_6^{c5}$ to give methylcyclopentadiene ($C_5H_6-CH_3$). The TST rate coefficient for this reaction is reported in Table 1. Successively, $C_5H_6-CH_3$ can get in an excited state through collisional energy transfer and form the adduct $C_6H_9^{c5*}$, which can successively react following the kinetic pathway outlined in Figure 12. Also in this case, the rate of formation of the products of the reaction were determined with QRRK theory. The results of the calculations, carried out using the TST rate coefficients of Table 1, are reported in Figure 13. Butadiene and C_2H_3 are the most stable species at high temperatures, while at lower temperatures, where collisional stabilization dominates, the $C_6H_9^{c5}$ and $C_6H_9^{l}$ adducts are the principal products. The QRRK rate coefficients interpolated between 300 and 2500 K at 1 and 0.01 atm are reported in Table 7. As in the previous case, three different conditions in which the adducts are or are not considered as products of the reaction have been considered. If the formation of the stabilized adducts is neglected, the rate of conversion of $C_5H_6-CH_3$ into $C_6H_8^{c6}$ and H increases significantly, thus becoming a viable alternative route of formation of *cyclo*-C_6 species.

4. Summary and Conclusions

The formation of the first aromatic ring plays an important role in defining the chemical reaction pathways responsible for

TABLE 6: QRRK Rate Coefficients for the Reactions of Addition of $C_6H_8^{c6}$ and H[a]

	$P = 1$ atm			$P = 0.01$ atm.		
reaction	$\log_{10} A$	α	E_a	$\log_{10} A$	α	E_a
	Products $C_2H_3 + C_4H_6$, $C_5H_6^{c5}$, $C_6H_8^{l}$					
$C_6H_8^{c6} + H \rightarrow C_2H_3 + C_4H_6$	35.5	−5.75	31 809	35.5	−5.75	31 809
$C_6H_8^{c6} + H \rightarrow C_5H_6^{c5} + CH_3$	34.6	−6.56	15 905	34.6	−6.56	15 905
$C_6H_8^{c6} + H \rightarrow C_6H_8^{l} + H$	29.9	−5.15	24 908	29.9	−5.15	24 908
	Products $C_2H_3 + C_4H_6$, $C_5H_6^{c5}$, $C_6H_8^{l}$, $C_6H_9^{c6}$, $C_6H_9^{c5}$					
$C_6H_8^{c6} + H \rightarrow C_2H_3 + C_4H_6$	43.66	−7.97	39 556	36.3	−5.98	32 478
$C_6H_8^{c6} + H \rightarrow C_5H_6^{c5} + CH_3$	55.4	−12.10	37 175	44.2	−9.18	24 021
$C_6H_8^{c6} + H \rightarrow C_6H_8^{l} + H$	41.2	−8.18	36 001	33.0	−5.98	27 313
$C_6H_8^{c6} + H \rightarrow C_6H_9^{c6}$	53.5	−12.20	20 055	55.4	−13.49	15 485
$C_6H_8^{c6} + H \rightarrow C_6H_9^{c5}$	73.1	−17.98	37 638	64.8	−16.46	25 557
	Products $C_2H_3 + C_4H_6$, $C_5H_6^{c5}$, $C_6H_8^{l}$, $C_6H_9^{c6}$, $C_6H_9^{c5}$, $C_6H_9^{l}$					
$C_6H_8^{c6} + H \rightarrow C_2H_3 + C_4H_6$	48.7	−9.32	44 550	36.6	−6.08	32 766
$C_6H_8^{c6} + H \rightarrow C_5H_6^{c5} + CH_3$	61.1	−13.64	43 870	45.6	−9.57	25 262
$C_6H_8^{c6} + H \rightarrow C_6H_8^{l} + H$	46.8	−9.67	41 952	33.7	−6.18	27 904
$C_6H_8^{c6} + H \rightarrow C_6H_9^{c6}$	53.5	−12.20	20 039	55.4	−13.49	15 485
$C_6H_8^{c6} + H \rightarrow C_6H_9^{c5}$	78.3	−19.32	45 021	67.0	−17.05	27 623
$C_6H_8^{c6} + H \rightarrow C_6H_9^{l}$	74.3	−17.89	40 691	66.7	−16.60	26 896

[a] Possible products were $C_2H_3 + C_4H_6$, $C_5H_6^{c5}$, $C_6H_8^{l}$, $C_6H_9^{c6}$, $C_6H_9^{c5}$, and $C_6H_9^{l}$. Values were fitted between 500 and 2500 K at 1 and 0.01 atm. $k = AT^{\alpha} \exp(-E_a/(RT))$. Preexponential factor and activation energies are reported in units consistent with kcal, s, mol, and cm.

TABLE 7: QRRK Rate Coefficients for the Reaction of Decomposition of $C_5H_6 - CH_3$ into $C_2H_3 + C_4H_6$, $C_5H_6^{c5}$, $C_6H_8^{l}$, $C_6H_9^{c6}$, $C_6H_9^{c5}$, and $C_6H_9^{l}$ Fitted between 500 and 2500 K at 1 and 0.01 atm, $k = AT^{\alpha}\exp(-E_a/(RT))$[a]

	$P = 1$ atm			$P = 0.01$ atm.		
reaction	$\log_{10} A$	α	E_a	$\log_{10} A$	α	E_a
	Products $C_2H_3 + C_4H_6$, $C_6H_8^{c6}$, $C_6H_8^{l}$					
$C_5H_6-CH_3 \rightarrow C_2H_3 + C_4H_6$	41.0	−7.30	79 826	41.0	−7.30	79 826
$C_5H_6-CH_3 \rightarrow C_6H_8^{c6} + H$	37.1	−7.38	63 305	37.1	−7.38	63 305
$C_5H_6-CH_3 \rightarrow C_6H_8^{l} + H$	39.7	−7.87	76 030	39.7	−7.87	76 030
	Products $C_2H_3 + C_4H_6$, $C_6H_8^{c6}$, $C_6H_8^{l}$, $C_6H_9^{c6}$, $C_6H_9^{c5}$					
$C_5H_6-CH_3 \rightarrow C_2H_3 + C_4H_6$	45.8	−8.62	84 055	41.2	−7.35	79 962
$C_5H_6-CH_3 \rightarrow C_6H_8^{c6} + H$	56.8	−12.77	81 000	40.2	−8.24	65 660
$C_5H_6-CH_3 \rightarrow C_6H_8^{l} + H$	46.5	−9.73	82 237	40.0	−7.97	76 304
$C_5H_6-CH_3 \rightarrow C_6H_9^{c6}$	77.1	−19.30	82 301	57.4	−14.56	62 950
$C_5H_6-CH_3 \rightarrow C_6H_9^{c5}$	51.1	−11.50	63 705	43.7	−10.20	53 266
	Products $C_2H_3 + C_4H_6$, $C_6H_8^{c6}$, $C_6H_8^{l}$, $C_6H_9^{c6}$, $C_6H_9^{c5}$, $C_6H_9^{l}$					
$C_5H_6-CH_3 \rightarrow C_2H_3 + C_4H_6$	51.85	−10.26	89 848	41.5	−7.43	80 188
$C_5H_6-CH_3 \rightarrow C_6H_8c6 + H$	65.3	−15.03	90 247	42.6	−8.90	67 558
$C_5H_6-CH_3 \rightarrow C_6H_8^{l} + H$	53.6	−11.60	89 372	40.6	−8.12	76 762
$C_5H_6-CH_3 \rightarrow C_6H_9^{c6}$	84.0	−21.06	91 751	60.6	−15.42	65 909
$C_5H_6-CH_3 \rightarrow C_6H_9^{c5}$	51.5	−11.60	64 042	43.7	−10.20	53 262
$C_5H_6-CH_3 \rightarrow C_6H_9^{l}$	78.1	−18.97	85 534	64.6	−16.11	67 182

[a] Preexponential factor and activation energies are reported in units consistent with kcal, s, mol, and cm.

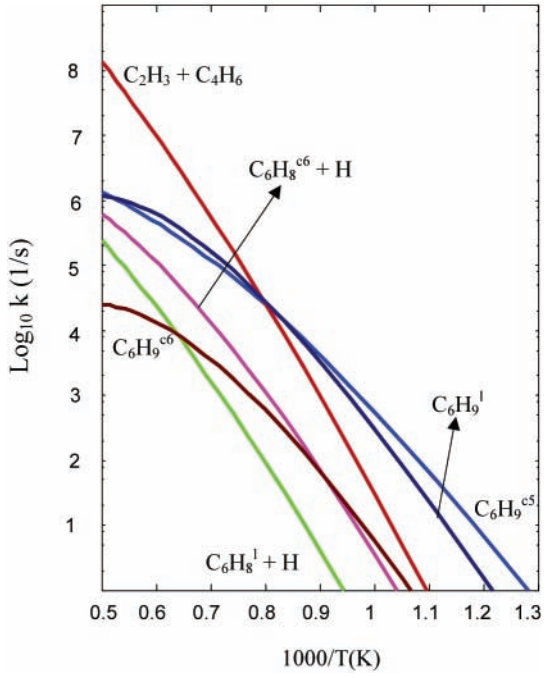

Figure 13. QRRK rate coefficients calculated for the decomposition of $C_5H_6-CH_3$ at 1 atm. All possible products were considered.

PAH and soot formation. A possible benzene formation channel involves the ethylene attack to cyclopentadiene, which in turn can be formed from the attack of vinyl radical on 1,3-butadiene. This reaction channel has been poorly investigated in the literature, and consequently, it is often disregarded in the proposed detailed kinetic schemes.

In this work, the relative importance of *cyclo*-C_5 species formation with respect to the *cyclo*-C_6 one has been studied through quantum Rice−Ramsperger−Kassel (QRRK) theory. Because of the lack of experimental information and to allow a fair comparison among different reaction channels, all of the relevant thermodynamic and kinetic parameters required by the QRRK approach have been estimated through quantum chemistry methods. A new approach, similar to that used in the G3 method to increase the accuracy of the calculated energies, has been used. It requires the optimization of the geometries of reactants, products, and transition states using the density functional theory, with correlation and exchange energies calculated with the B3LYP functionals and the 6-31G(d,p) basis set, while the energy of each molecule is calculated using a procedure similar to that adopted in the G2MP2 method. In other words, this approach differs from the standard G2MP2 method in that geometries were optimized with B3LYP/6-31G(d,p).

This allows for a faster yet accurate estimation of the kinetic parameters. The reliability of this approach for the reactions involved in this study has been estimated by comparing its predictions both with the prediction of other methods and, when available, with some experimental results. It has been found that its results are always comparable and usually better than that of B3LYP/6-31G(d,p), QCISD(T)/6-311+G(d,p), MP2/6-311+G(3df,2p), and MP2/6-311+G(d,p) for what concerns the prediction of the reaction enthalpy change. Moreover, when considering a similar reaction (that is, the addition of C_2H_3 to C_3H_6), a good agreement (that is, inside the experimental uncertainty) has been found between model predictions and experimental data.

Using this approach, we performed a detailed analysis of the reaction paths following the addition of C_2H_3 to C_4H_6 to form the hexadienyl radical. The overall reaction rates of the various reaction patterns leading to *cyclo*-C_5 and -C_6 species depend on the other species considered in the reaction network. However, it has been always found that the rate of formation of $C_5H_6^{c5}$ is larger than that of $C_6H_8^{c6}$ in the whole temperature range investigated (that is, 500−2000 K). Moreover, the kinetic constant values estimated can account for some experimental evidences referring to benzene formation rate, as well as the relative abundance of *cyclo*-C_5 or -C_6 species.

Finally, also the rates of the reactions from the *cyclo*-C_5 or -C_6 species back to other species involved in the reaction network have been estimated. This gives an idea of the reactivity of these species once formed. A channel for the conversion of $C_5H_6^{c5}$ into $C_6H_8^{c6}$, passing through the addition of CH_3, was identified, and QRRK rate coefficients were calculated. This provides a further route of formation of benzene through *cyclo*-C_5 species.

All of these results lead to the conclusion that the reaction paths involving *cyclo*-C_5 species cannot be neglected in the detailed kinetic modeling of combustion processes when the first aromatic ring formation is involved.

Acknowledgment. The authors are indebted with Proff. E. Ranzi and T. Faravelli for continuous and fruitful discussions.

References and Notes

(1) Beer, J. M. *Prog. Energy Combust. Sci.* **2000**, *26*, 301.
(2) Siegmann, K.; Siegmann, H. C. Molecular precursor of soot and quantification of the associated health risk. In *Current problems in condensed matter*; Morán-Lopez, J. L., Ed.; Plenum Press: New York, 1998; pp 143−160.
(3) Richter, H.; Howard, J. B. *Prog. Energy Combust. Sci.* **2000**, *26*, 565.
(4) D′Alessio, A.; D′Anna, A.; Minutolo, P.; Sgro, L. A.; Violi A. *Proc. Combust. Inst.* **2000**, *28*, 2547.
(5) Cole, J. A.; Bittner, J. D.; Longwell, J. P., Howard, J. B *Combust. Flame* **1984**, *56*, 51.
(6) Frenklach, M.; Warnatz, J. *Combust. Sci. Technol.* **1987**, *51*, 265.
(7) Lindstet, R. P.; Skevis, G. *Proc. Combust. Inst.* **1996**, *26*, 703.
(8) Dente, M.; Ranzi, E.; Goossens, A. G. *Comput. Chem. Eng.* **1979**, *3*, 61.
(9) Miller, J. A.; Melius, C. F. *Combust. Flame* **1992**, *91*, 21.
(10) Dente, M.; Ranzi, E. Mathematical modeling of hydrocarbon pyrolysis reactions. In *Pyrolysis: Theory and industrial practice*; Lyle, F., Crynes, B. L., Corcoran, W. H., Eds., Academic: New York, 1983; pp 133−175.
(11) Goldaniga, A.; Faravelli, T.; Ranzi, E. *Combust. Flame* **2000**, *122*, 350.
(12) Westmoreland, P. R.; Dean, A. M.; Howard, J. B.; Longwell, J. P. *J. Phys. Chem.* **1989**, *93*, 8171.
(13) Dean, A. M. *J. Phys. Chem.* **1985**, *89*, 4600.
(14) Violi, A.; Sarofim, A. F.; Truong, T. N. *Combust. Flame* **2001**, *126*, 1506.
(15) Sumathi, R.; Carstensen, H.-H.; Green, W. H., Jr. *J. Phys. Chem. A* **2001**, *105*, 6910.
(16) Troe, J. *J. Chem. Phys.* **1977**, *66*, 4745.
(17) (a) Becke, A. D. *J. Chem. Phys.* **1993**, 98, 5648. (b) Lee, C.; Yang, W.; Parr, R. G. *Phys. Rev. B* **1988**, *37*, 785.
(18) Curtiss, L. A.; Raghavachari, K.; Pople, J. A. *J. Chem. Phys.* **1995**, *103*, 4192.
(19) Curtiss, L. A.; Redfern, P. C.; Raghavachari, K.; Pople, J. A. *J. Chem. Phys.* **2001**, *114*, 108.
(20) Hirschfelder, J. O.; Wigner, E. *J. Chem. Phys.* **1939**, *7*, 616.
(21) Frisch, M. J.; Trucks, G. W.; Schlegel, H. B.; Scuseria, G. E.; Robb, M. A.; Cheeseman, J. R.; Zakrzewski, V. G.; Montgomery, J. A., Jr.; Stratmann, R. E.; Burant, J. C.; Dapprich, S.; Millam, J. M.; Daniels, A. D.; Kudin, K. N.; Strain, M. C.; Farkas, O.; Tomasi, J.; Barone, V.; Cossi, M.; Cammi, R.; Mennucci, B.; Pomelli, C.; Adamo, C.; Clifford, S.; Ochterski, J.; Petersson, G. A.; Ayala, P. Y.; Cui, Q.; Morokuma, K.; Malick, D. K.; Rabuck, A. D.; Raghavachari, K.; Foresman, J. B.; Cioslowski, J.; Ortiz, J. V.; Stefanov, B. B.; Liu, G.; Liashenko, A.; Piskorz, P.; Komaromi, I.; Gomperts, R.; Martin, R. L.; Fox, D. J.; Keith, T.; Al-Laham, M. A.; Peng, C. Y.; Nanayakkara, A.; Gonzalez, C.; Challacombe, M.; Gill, P. M. W.; Johnson, B. G.; Chen, W.; Wong, M. W.; Andres, J. L.; Head-Gordon, M.; Replogle, E. S.; Pople, J. A. *Gaussian 98*, revision A.6; Gaussian, Inc.: Pittsburgh, PA, 1998.
(22) Gilbert, R. G.; Smith, S. C. *Theory of Unimolecular and Recombination Reactions*; Blackwell Scientific Publications: Oxford, U.K., 1990.
(23) Furukawa, K.; James, D. G. L.; Papic, M. M. *Int. J. Chem. Kinet.* **1974**, *6*, 337.
(24) Van Speybroeck, V.; Van Neck, D.; Waroquier, M.; Wauters, S.; Saeys, M.; Marin, G. B. *J. Phys. Chem. A* **2000**, *104*, 10939.
(25) Tsang, W.; Hampson, R. F. *J. Phys. Chem. Ref. Data* **1987**, *15*, 887.
(26) Reid, R. C.; Prausnitz, J. M.; Poling, B. E. *The Properties of Gases and Liquids*; McGraw-Hill: New York, 1987.
(27) Cole, J. A.; Bittner, J. D.; Longwell, J. P.; Howard J. B. *Combust. Flame* **1984**, *56*, 51.
(28) Benson, S. W.; Shaw, R. *Trans. Faraday Soc.* **1967** *63*, 985.
(29) Brezinsky, K.; Burke, E. J.; Glassman, I. *Proc. Combust. Inst.* **1984**, 613.
(30) *CRC Handbook of Chemistry and Physics*; Lide, D. R., Ed.; CRC Press: Boca Raton, FL, 1996.